FISEVIER

Contents lists available at ScienceDirect

International Journal of Plasticity

journal homepage: www.elsevier.com/locate/ijplas





Crystal plasticity modeling of ultrasonic softening effect considering anisotropy in the softening of slip systems

Jiarui Kang^a, Xun Liu^{a,*}, Stephen R. Niezgoda^{b,c}

- ^a Welding Engineering, Department of Material Science and Engineering, The Ohio State University, Columbus, OH, 43221, USA
- b Material Science and Engineering, Department of Material Science and Engineering, The Ohio State University, Columbus, OH, 43221, USA
- ^c Mechanical Engineering, Department of Mechanical and Aerospace Engineering, The Ohio State University, Columbus, OH, 43221, USA

ARTICLE INFO

Keywords: Ultrasonic softening Crystal plasticity VPSC Taylor factor Texture

ABSTRACT

In this study, a novel approach to modeling the ultrasonic softening effect during metal plasticity is developed, where the slip systems experience differential softening depending on their orientation relative to the ultrasonic direction. The directional softening model was implemented within a Visco-Plastic Self-Consistent (VPSC) model, where the material and ultrasonic softening parameters are calibrated based on micro-tensile test data of pure copper with tension along the rolling direction of sheet. The model is then validated against the stress-strain response of the samples with tension along transverse direction. The VPSC modeling results provide new insights into ultrasonic softening, particularly that the stress reduction is not homogeneous in the whole aggregate. The degree of softening shows a strong dependence on grain orientation. A higher level of stress reduction is observed in plastically hard, high Taylor factor grains. A decrease in Taylor factor is predicted, especially in the grain subset with higher stress reduction, which agrees with experimental data. Although a traditional isotropic softening model is also capable in predicting the ultrasonically softened stress-strain response for different texture inputs, this decrease in Taylor factor cannot be captured.

1. Introduction

Acoustic softening describes the phenomenon that superimposed ultrasonic vibrations, with a frequency of 20–100 kHz and amplitude around 1–30 µm, can effectively reduce the material flow stress during plastic deformation (Graff, 2015). A considerable number of experimental studies with ultrasonic assisted (UA) deformation have been performed. Dutta et al. conducted UA tensile tests on low-carbon steel and reported the reduction of dislocation density and low angle grain boundary (Dutta et al., 2013). Similar result has also been reported by Wang et al. when they performed small scale tension tests with UA on pure titanium (Wang et al., 2021). The modification of deformation microstructure and the reduction in dislocation density is generally attributed to enhanced dislocation motion under UA. Under additional oscillatory stress, dislocations travel longer distances and therefore the chance for annihilation is higher (Siu and Ngan, 2011; Yao et al., 2012). In addition to the change in dislocation density, effects of UA on grain rotation have also been reported. Zhou et al. studied UA compression of aluminum and observed reduced Taylor factor with UA, indicating grain re-orientation towards easier slip conditions (Zhou et al., 2018). Weaker texture in ultrasonic consolidation was reported and attributed to different grain rotation rates with UA (Mariani and Ghassemieh, 2010; Siddig and Sayed, 2012a). However, in the case of

E-mail address: liu.7054@osu.edu (X. Liu).

^{*} Corresponding author.

ultrasonic consolidation, extensive shear and heat generation can mask the intrinsic UA effect on material deformation. Further investigation with modeling analysis is needed in this area to better understand the mechanism of ultrasonic softening and examine UA effect on grain rotation.

To quantify the stress reduction associated with ultrasonic energy, two general modeling approaches have been explored: 1) explicit simulation through stress superposition and 2) modifications of constitutive theories which implicitly consider the additional ultrasonic energy input. The stress superposition approach directly simulates the ultrasonic effects by applying boundary conditions with either high frequency alternating loads (Malygin, 2000) or displacement (Graff, 2015; Zhuang et al., 2015). However, the assumption that material behavior stays unchanged does not agree with the experimental evidence of microstructural change under ultrasonic vibration. To account for this, more physics-based models that modify material constitutive behavior have been proposed. These models explicitly consider the deformation mechanisms and microstructure evolution at multiple length scales, spanning from nano-scale dislocation movement, through micro-scale grain deformation and rotation, finally to the macro-scale effective stress-strain relationships. Commonly used ultrasonic parameters include acoustic energy intensity and density (Mao et al., 2020; Wang et al., 2016), as expressed in the following equations:

Acoustic energy intensity
$$I_{UA} = 2\pi^2 f^2 A^2 \sqrt{E\rho_m}$$
 (1)

Acoustic energy density
$$\xi_{UA} = 4\pi^2 f^2 A^2 \rho_m = \frac{p_{UA}^2}{2\rho_m c^2}$$
 (2)

where f is the frequency, A is the vibration amplitude, and ρ_m is the material density, p_{UA} is the local acoustic pressure, and c is the sound velocity in the material.

Siddiq and Sayed (2012b, 2011) employed a crystal plasticity modeling approach and introduced a softening coefficient U_{soft} to the strength of slip system as:

$$\dot{\gamma}^a = \dot{\gamma}^0 \operatorname{sgn}(\tau^a) \left\{ \left| \frac{\tau^a}{g^a \cdot U_{soft}} \right| \right\}^n \tag{3}$$

where $\dot{\gamma}^{\alpha}$ and g^{α} are the plastic strain rate and the strength of the slip system α respectively, and n is the rate-sensitivity factor. The softening coefficient U_{soft} is a function of ultrasonic intensity I_{UA} and is expressed as:

$$U_{\text{soft}} = (1 - d_{ut} \cdot I_{t/A})^{\epsilon_{ut}} \tag{4}$$

where d_{ut} and e_{ut} are ultrasonic softening material parameters. Yao et al. (2012) employed a dislocation density based crystal plasticity model, where the ultrasonic density is incorporated into the stress reduction and dislocation evolution terms explicitly. The stress reduction ratio $\Delta \lambda$ is related to dislocation density ρ and acoustic energy density ξ_{UA} by:

$$\Delta \lambda = \frac{\Delta \tau}{\widehat{\tau}} = -\beta \left(\frac{\xi_{UA}}{\widehat{\tau}} \right)^m = -\beta \left[\frac{\xi_{UA}}{\left(\tau_0 + \mu \alpha b \sqrt{\rho} \right)} \right]^m \tag{5}$$

where τ_0 and α are material parameters, μ is friction coefficient, b is the Burgers vector of a dislocation. The evolution of the dislocation density, ρ , can be determined by:

$$\frac{d\rho}{d\nu} = k_1 (1 + \eta_{k1}) \sqrt{\rho} - k_{20} \left(\frac{\dot{\varepsilon}}{\dot{\varepsilon}_0}\right)^{-\frac{1}{n}} (1 + \eta_{k2}) \rho \tag{6}$$

where γ is the shear plastic strain, k_{20} , $\dot{\varepsilon}_0$, k_1 are the material related parameters, η_{k2} and η_{k1} correspond to the ultrasonically induced dislocation multiplication and annihilation, respectively. Both ultrasonically induced residual softening, and hardening effects can be effectively captured by modifying these coefficients. η_{k1} can be further expressed by the ultrasonic vibration amplitude A as:

$$\eta_{k1} = \frac{C_4 P_0}{[P_0 + (C_4 - P_0)e^{\phi A}]} \tag{7}$$

where C_4 , P_0 and ϕ are material parameters. This model has been adopted by Bagherzadeh and Abrinia (2015) to quantify the softening and residual hardening during ultrasonically assisted compression of pure aluminum. Cao et al. (2020) also applied this model in comparing the relative significance of ultrasonic volume softening and surface frictional effects in the upset force reduction for AA 6061. Deshpande and Hsu (2018) adopted a modified Kocks-Mecking-Estrin model to account for the ultrasonically induced dynamic recovery, where the activation energy for dislocation annihilation is reduced by a coefficient with acoustic energy density ξ_{UA} , as in:

$$\frac{d\rho}{d\gamma} = -k_{20} \left(\frac{\dot{\varepsilon}}{\dot{\varepsilon}_{0}^{*}}\right)^{-\frac{1}{n}} \rho \tag{8}$$

and $\dot{\varepsilon}_0^*$ is expressed with an ultrasonically modified Arrhenius equation:

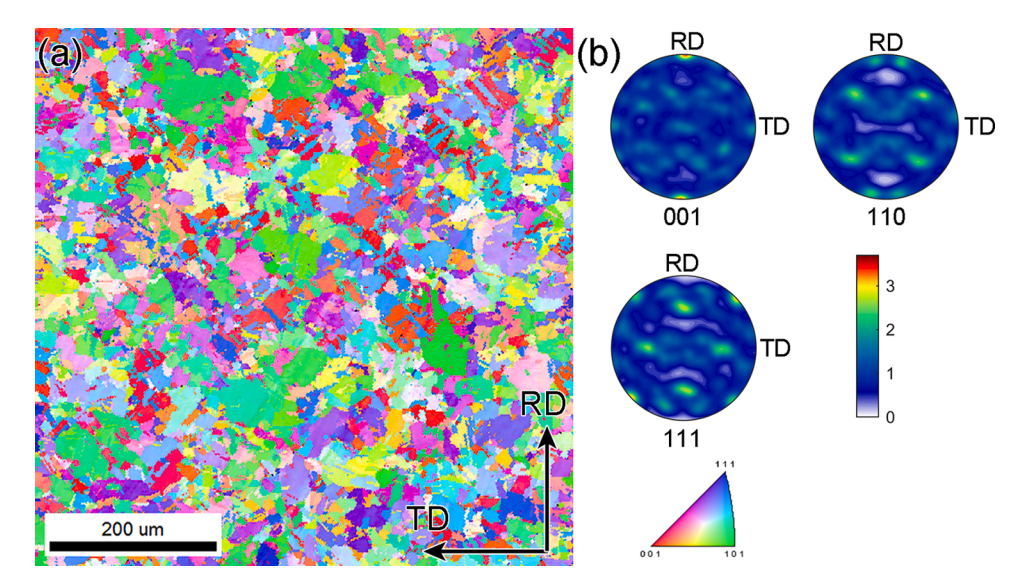


Fig. 1. EBSD characterization of the as-received copper foil (a) orientation distribution map; (b) {001}, {110} and {111} pole figures showing a superposition of typical FCC rolling and annealing textures.

$$\dot{\varepsilon}_0^* = \dot{\varepsilon}_{00}^* \exp\left(\frac{-C_5 Q_d}{k_B T \xi_{IIA}}\right) \tag{9}$$

where Q_d is the activation energy for self-diffusion, T is temperature, and C_5 is an adjustable coefficient. Wang et al. (2021) discussed an ultrasonically induced reduction of the Hall-Petch slope as a result of heterogeneous modification of dislocation dynamics at the microstructure level and alleviation of dislocation emission resistance across grain boundaries. They incorporated a generic power function of acoustic energy density in changing the dislocation annihilation and storage coefficients. Prabhakar et al. (2017) incorporated ultrasonic energy as a modification term ΔQ_{UA} on the activation energy:

$$\dot{\varepsilon} = \dot{\varepsilon}_0 \exp\left(\frac{-(\Delta Q + \Delta Q_{UA})}{k_B T}\right) \tag{10}$$

The dislocation density ρ can be incorporated into ΔQ_{UA} by Yang and Wu (2019),

$$\Delta Q_{UA} = \frac{C_1 \Delta F}{k_B} \left(\frac{\xi_{UA}}{\tau_0 + \mu a b \sqrt{\rho}} \right)^m \tag{11}$$

where ΔF is the change of Helmholtz free energy, k_B is the Boltzmann constant. Sedaghat et al. (2019) considered the Gibbs free energy ΔG_s required for plastic deformation as the summation of the Helmholtz free energy change for dislocation motion, ΔF , and the additional acoustic work W. The acoustic work, W, is the product of acoustic stress σ_{UA} and effective activation volume V (Choi et al., 2014). A similar approach was also taken by Zhao and Wu (2019):

$$W = \sigma_{UA}V = \left(-\frac{E}{2\pi f}\frac{dv}{dr}\right)\sqrt{3}k_BT\left[\frac{\partial\ln(\dot{\varepsilon})}{\partial\sigma}\right]$$
(12)

where $\dot{\varepsilon}$ is strain rate and σ is stress. The acoustic stress σ_{UA} can be written as:

$$\sigma_{UA} = \sqrt{2\eta\pi}f\rho_m cA$$
 (13)

where η is an efficiency factor.

One implicit assumption used in these models is that the effect of UA is assumed to be identical among different slip systems. This might not be physically accurate as the softening effect could be related to the orientation relationship between slip system and oscillation direction. For example, dislocation glide would be most significantly facilitated when slip system is aligned with UA direction. In contrast, minimal effect is expected if slip system is perpendicular to applied UA. In present work, an orientation-dependent softening model is proposed to bridge this gap, and to better understand the UA effect on polycrystal material where orientation varies from grain to grain. The directionality effect of UA, while not addressed before, could also help explain the discrepancy in UA effect on microstructural change with different ultrasonic direction. For example, an enhancement of subgrain formation is reported in BCC molybdenum and FCC aluminum when the ultrasonic vibration is transverse to the compression direction (Siu et al., 2011; Siu and Ngan, 2013). Contradictorily, a reduction of subgrain formation is observed in BCC low carbon steel when the ultrasonic vibration is

along the static loading direction (Dutta et al., 2013). In this study, a new directional acoustic softening modeling approach is established within the visco-plastic self-consistent (VPSC) framework. This model is phenemonolgical in nature but successfully explains several features of ultrasonic softening which has not been addressed in the previous literature. The model is validated against ultrasonically assisted micro-tensile tests of pure copper in different loading directions.

2. Experimental procedure

2.1. Materials and characterization

Commercially available electrolytic tough pitch copper (purity of 99.9%) was used in this study. The as-received copper foils had a thickness of 200 μ m and were in the tempered annealed condition. Characterization by Electron Backscatter Diffraction (EBSD, see below) shows a microstructure with relatively equiaxed grains with an average grain size of approximately 9.3 μ m, as shown in Fig. 1 (a). Texture analysis as shown in {001}, {110} and {111} pole figure (see Fig. 1(b)), reveals a mixture of rolling and annealing texture in the as-received copper foils.

EBSD characterization was performed on an FEI Apreo field emission scanning electron microscope equipped with EDAX Hikari EBSD detector at a 20 mm working distance, 13 nA beam current, and 20 kV accelerating voltage. The sample was tilted 70° to horizontal axis and a step size of $1.5 \, \mu m$ was used for all scans. On deformed specimens without and with ultrasonic assistance, three regions were scanned on the gage section and stitched together for analysis. This ensures that a larger number of grains are sampled for texture analysis. Grain reconstruction was performed in Orientation Imaging Microscopy (OIM) software using a grain tolerance angle of 5° and a minimum grain size of 2 pixels. All texture analysis was performed using MTEX toolbox (Hielscher and Schaeben, 2008). Pole figures were plotted from a discrete orientation distribution function (ODF) fitted to de La Vallée Poussin kernel with a half-width of 5°

2.2. Micro-tensile testing

Micro-tensile tests were performed to investigate the plastic behavior of pure copper and the effect of ultrasonic vibration. The main advantage of testing small scale samples is that the variation of ultrasonic amplitude along sample gage is minimal. This is because the gage length of 1.7 mm is more than an order of magnitude smaller relative to the longitudinal ultrasonic wavelength in copper:

$$\lambda = 1/f\sqrt{E/\rho} = 18.3 \text{ cm} \tag{14}$$

where f is ultrasonic frequency 20 kHz, E and ρ are the elastic modulus and density of pure copper and are 119 GPa and 8.9 g/cm³, respectively (Maloney et al., 2013). Dogbone specimens were placed into grips with matching geometry. One grip is connected to a high-resolution linear actuator while the other is mounted to an ultrasonic transducer which vibrates along the tensile direction. A schematic of the setup and further details are given in Reference (Kang et al., 2020). Dogbone specimens were machined by wire electrical discharge machining with one initial cut and two skim cuts that use progressively less energy to achieve a surface finish of Ra 0.4 μ m. Two sets of specimens with tensile directions oriented along the rolling direction (RD) and transverse direction (TD) of the rolled foil were prepared. Prior to testing, specimens were polished using 3 μ m and 1 μ m diamond paste, followed by vibratory polishing using 0.02 μ m colloidal silica. Specimens tested to 17% strain in different conditions were analyzed by EBSD. 17% strain was chosen based on the observation from digital image correlation that strain distribution is uniform along sample gage. This minimizes error in texture analysis that could be induced by local strain variation when stitching multiple EBSD scans collected along gage section. Three samples were tested at each condition and texture.

3. Modeling the direcitonal ultrasonic effect

The ultrasonic softening models described in this section were implemented in the Visco-Plastic Self-Consistent (VPSC) solver developed by Lebensohn and Tomé (1993). VPSC is a mean-field crystal plasticity model that treats grains as inclusions embedded in a visco-plastic medium and calculates plastic deformation from slip and twinning systems activation under resolved deviatoric shear stress.

In the earlier crystal plasticity model proposed by Siddiq and Sayed (2011), the microscopic flow rule was modified so that the strength of all slip systems was scaled down by the same factor when UA was applied. A similar isotropic softening scheme has also been employed by Choi et al. (2014) and Zhao and Wu (2019) where the work of acoustic stress is incorporated in activation energy for dislocation motion. The additional work done by ultrasonic vibration is expressed as $W = \sigma_{UA}V$, where σ_{UA} is acoustic stress and V is activated volume. On the other hand, if the ultrasonic effect is considered from the perspective of acoustic stress, which is a second order tensor, its relative direction with regard to the slip systems should be incorporated. The governing rules should be similar to those of the externally applied stress. The force on a dislocation from an acoustic stress field can be written following the Peach–Koehler equation (Peach and Koehler, 1950): $f = (\sigma_{UA} \cdot b) \times \xi$, where b is Burgers vector and ξ is the line direction of a dislocation. This suggests that the degree of softening is different depending on the relative orientation between the slip system and acoustic stress. Physically it is interpretable that dislocation glide will be facilitated most effectively when ultrasonic vibration is aligned along the slip direction, while the softening effect is minimized when ultrasonic vibration is perpendicular to the slip direction. In other words, the softening effect of UA is not isotropic amongst the different slip systems. It can be hypothesized that only the

Table 1 VPSC parameters used in modeling.

	$\tau_0(MPa)$	τ ₁ (MPa)	θ_0 (MPa)	θ_1 (MPa)	a_0	A(μm)	d(μm)
No UA	39.0	98.0	260.0	25.0	-	_	-
UA	32.0	98.0	260.0	25.0	0.01788	1.3	9.3

component decomposed onto the slip plane and along the slip direction, can facilitate dislocation glide. Similar to the decomposition of external stress, this directional softening effect of acoustic stress relative to the slip system can be expressed via an inner product of the Schmid tensor for the system and the acoustic stress tensor. Accordingly, the rate-sensitive viscoplastic law is proposed to be modified as:

$$\dot{\gamma}^{a} = \dot{\gamma}_{0} \operatorname{sgn}(\sigma^{a}) \left\{ \left| \frac{\sigma^{a}}{k^{a} \cdot \hat{\tau}^{a}} \right| \right\}^{n}$$
(15)

where $\dot{\gamma}^a$ and $\dot{\gamma}_0$ are the plastic and reference strain rate in the slip system α , σ^a and $\hat{\tau}^a$ are the resolved shear stress and the original critical resolved shear stress (CRSS) of the slip system α , n is the rate-sensitivity factor. The softening coefficient k^a is formulated considering the relative orientation between the direction of ultrasonic vibration and slip system with Schmid matrix M^a , and is expressed as:

$$k^a = 1 - a|\mathbf{M}^a: U| \tag{16}$$

where a is the parameter describing the degree of softening, U is a tensor characterizing the directionality of acoustic stress, which coincides with the direction of ultrasonic wave propagation (Dukhin and Goetz, 2017). U is expressed as:

$$U = \begin{pmatrix} 0 & 0 & 0 \\ 0 & 0 & 0 \\ 0 & 0 & 1 \end{pmatrix} \tag{17}$$

when ultrasonic vibration is applied along the third axis. The magnitude of acoustic stress on individual grains is assumed to be the same and is incorporated in softening coefficient a. In each individual grain, $|M^a:U|$ gives the absolute value of the component of ultrasonic vibration acting on slip system α . The larger this value is, the more effective the change in CRSS will be. The evolution of CRSS is formulated using Voce hardening law and is expressed as:

$$\widehat{\tau} = \tau_0 + (\tau_1 + \theta_1 \Gamma) \left(1 - \exp\left(-\Gamma \frac{\tau_0}{\tau_1} \right) \right) \tag{18}$$

where Γ is the accumulated shear strain in grain, τ_0 , θ_0 , θ_1 , and $(\tau_0 + \tau_1)$ are the initial CRSS, the initial hardening rate, the asymptotic hardening rate, and the back-extrapolated CRSS for slip systems.

The introduction of a directional softening factor k^{α} lowers the CRSS of individual slip systems under UA. We further propose that the hydrostatic component of the long wavelength oscillating UA stress also contributes a smaller (relative to the directional softening) isotropic softening. This hypothesis is motivated by the experimental observation that UA lowers both the yielding strength and plastic flow stress of materials (Fartashvand et al., 2017; Graff, 2015). This isotropic component corresponds to a decrease in the activation barrier to slip, while the directional softening factor accounts for the increase in energy available to activate slip. To incorporate the effect of this isotropic softening with VPSC, which by design only considers the deviatoric stress state, the initial yield Voce hardening parameter, τ_0 , is also adjusted lower to reflect the change in initial yield point (See Table 1).

It is assumed that acoustic energy is preferentially absorbed in microscopic defects such as dislocations and grain boundaries and that dislocations can move faster and break away from obstacles more easily (Siu and Ngan, 2011; Zhao and Wu, 2019). The degree of softening depends on the ultrasonic process parameters and initial material microstructure. It is reported that the flow stress reduction is proportional to the vibration amplitude (Bagherzadeh and Abrinia, 2015; Wang et al., 2016; Yao et al., 2012). In addition, a stronger softening effect was observed in smaller grains under the same ultrasonic condition (Wang et al., 2021). Considering these factors, the softening parameter a is formulated as:

$$a = a_0 \frac{A}{d} \tag{19}$$

where A is the vibration amplitude, d is the average grain size, and a_0 is a parameter obtained from fitting.

In order to clarify the role of directional softening, a purely isotropic model was also set up, where ultrasonic softening is assumed to be isotropic, i.e., the level of reduction in CRSS is the same for all slip systems. In the isotropic softening model, the modified microscopic flow rule follows the same form as Eq. (15) except that k is a constant and does not change with respect to slip system orientation.

All crystal plasticity simulations were performed in VPSC7d, with the same mixed boundary condition for tensile deformation along the third axis:

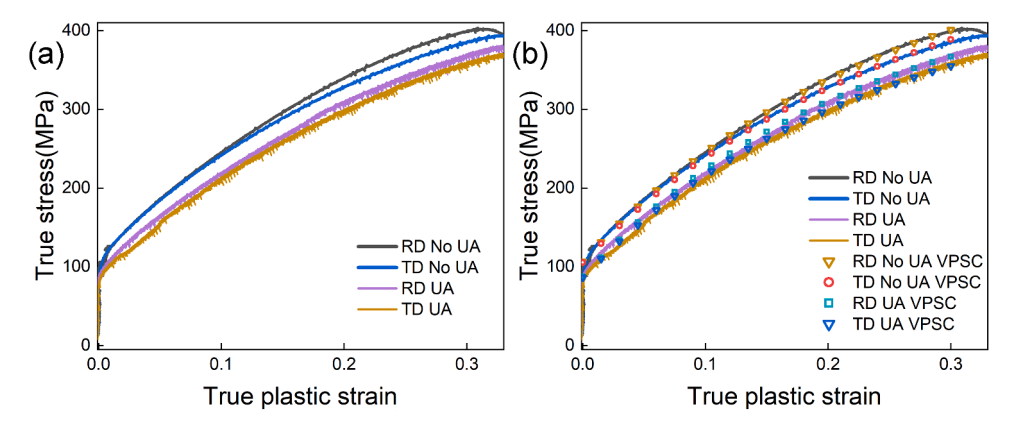


Fig. 2. True stress-strain results on micro-tensile tests of pure copper (a) experimental and (b) with VPSC results overlay.

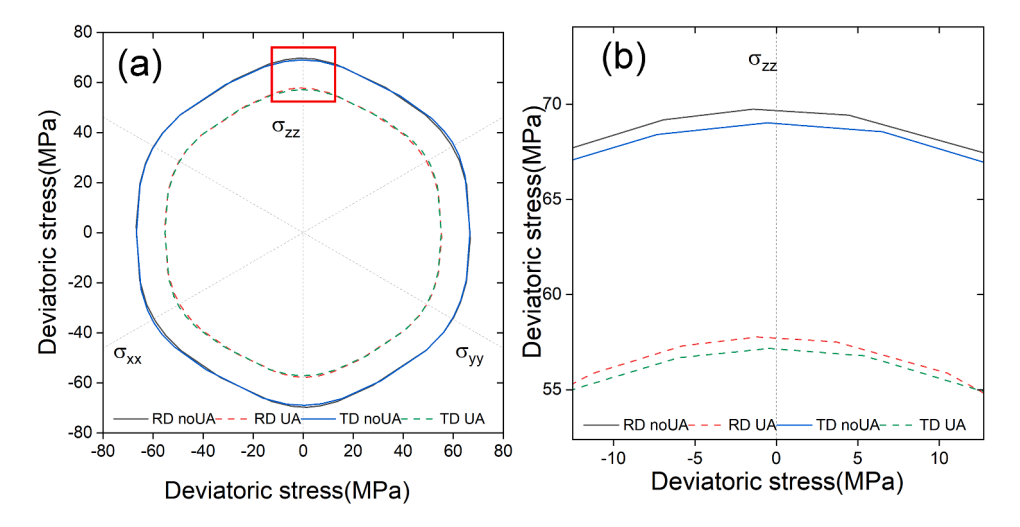


Fig. 3. VPSC yield surface results for micro-tensile test on (a) pure copper with and without UA and (b) zoomed-in view on region marked by red square.

$$\mathbf{L} = \begin{pmatrix} L_{11} & 0 & 0 \\ 0 & L_{22} & 0 \\ 0 & 0 & 1 \end{pmatrix} \tag{20}$$

$$\boldsymbol{\sigma} = \begin{pmatrix} 0 & \sigma_{12} & \sigma_{13} \\ \sigma_{12} & 0 & \sigma_{23} \\ \sigma_{13} & \sigma_{23} & \sigma_{33} \end{pmatrix} \tag{21}$$

where L and σ are velocity gradient tensor and Cauchy stress tensor, respectively. Deformation modes were set as $\langle 111 \rangle$ {110} slip. The self-consistent problem was linearized using n_{eff} =10 method as described by Lebensohn and Tomé (2015) since it produces the most stable behavior (Sridhar et al., 2022). For simplicity, initial grain shape was set to spherical, and grain co-rotation was not activated.

4. Results

4.1. Ultrasonically assisted micro-tensile test and VPSC prediction

Fig. 2(a) shows the true stress-strain curves obtained from micro-tensile tests on pure copper. The tests with UA applied along the tensile direction are compared with the conventionally tested samples in both RD and TD specimens. Samples tested with UA show a lower yield point and reduced flow stress during plastic deformation. At 17% true strain, the stress reduction in the RD and TD samples are 31.8 MPa and 27.5 MPa, respectively. Because of the anisotropy in texture, as seen in Fig. 1(b), TD specimens show a lower flow

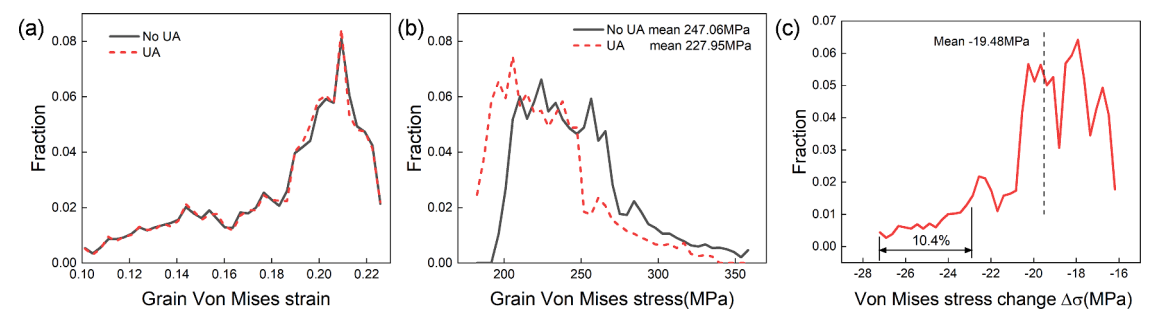


Fig. 4. Distribution of grain level (a) Von Mises strain; (b) Von Mises stress; and (c) change in Von Mises stress of simulated TD test at 17% strain.

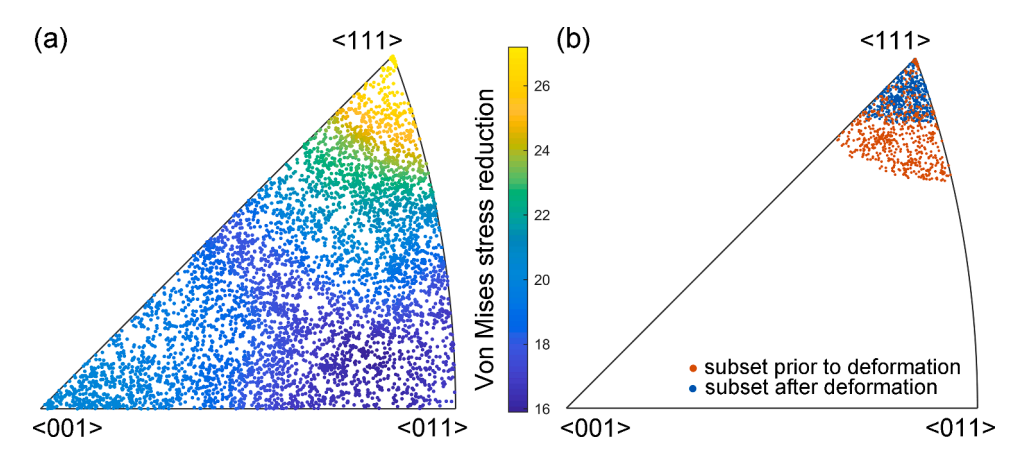


Fig. 5. Discrete orientation of (a) initial texture along TD direction, color coded by Von Mises stress reduction; (b) $\langle 111 \rangle$ subset prior to and after tensile deformation.

stress than the RD samples; both in conventional and UA condition. Furthermore, the UA induced stress reduction in TD samples is also larger

A VPSC model using Voce hardening was calibrated on the RD samples and then validated against the TD experimental stress-strain curves. For the VPSC simulations, 5190 grain orientations, extracted from EBSD, are used as the input texture. First, the VPSC model is calibrated with the conventional tensile tested stress-strain curve from a RD sample tested without UA. The obtained Voce parameters are listed in Table 1. Second, the softening parameter a_0 in the ultrasonic term is obtained by fitting the true stress-strain curve of RD samples tested with UA. According to the experimental configuration, the ultrasonic vibration amplitude A is 1.3 μ m and the average grain size d is 9.3 μ m. τ_0 is the initial CRSS of a crystal and is adjusted lower by 7 MPa. The model is then applied to TD tests as a validation, with all parameters kept the same while only rotating the input texture. Results from the VPSC model are overlayed on experimental data and are shown in Fig. 2(b). In both conditions, without and with UA, the VPSC model prediction matches well with the stress-strain data of the TD specimens; successfully capturing the reduction of flow stress and the plastic anisotropy when compared with the UA test on RD samples.

Based on this developed VPSC model, polycrystal yield surfaces for the initial texture were calculated. Fig. 3(a) shows the π -plane projection in the deviatoric stress space (Lebensohn and Tomé, 2015), with the region marked with a red rectangle zoomed-in and plotted in Fig. 3(b). In both RD and TD simulations, yield surfaces with UA, shown with dashed lines, shrinks considerably compared with the conventionally tested ones, shown in solid lines. The yield points of RD and TD samples with UA are both lower than the ones without UA. This matches with experimental observations that specimens are easier to yield with applied ultrasonic vibration. When comparing between RD and TD specimens, the yield point of RD sample is higher than the TD sample in both UA and no UA conditions. This is attributed to the anisotropy in texture (Rout, 2020). As shown in Fig. 6(a), higher intensities in $\langle 111 \rangle$ is observed in RD sample. These grains have high Taylor factors, and this leads to a higher strength (Groche et al., 2010).

Statistical analyses were performed on the distribution of grain Von Mises strain and stress, based on the simulated TD test at 17% strain. The resulting histograms are shown in Fig. 4(a) and (b). No significant change due by UA is observed in grain Von Mises strain. This matches with the identical macroscopic strain path applied in both UA and no UA conditions. In contrast, while the trend of Von Mises stress distribution remains similar, a noticeable shift of the curve towards lower values is observed with UA, as shown in Fig. 4(b). The average of Von Mises stress decreases from 247.06 MPa to 227.95 MPa with ultrasonic application. To understand the effect of UA on a grain level, the change of Von Mises stress induced by UA on individual grain is calculated as $\Delta \sigma = \sigma_{VM}^{VA} - \sigma_{VM}^{NO~UA}$ and the histogram is plotted in Fig. 4(c). All grains exhibit a negative value in stress change, which indicates that stress reduction is happening in every grain. It is worth noting that the magnitude of stress reduction is not homogenous in the simulated aggregate. While a large

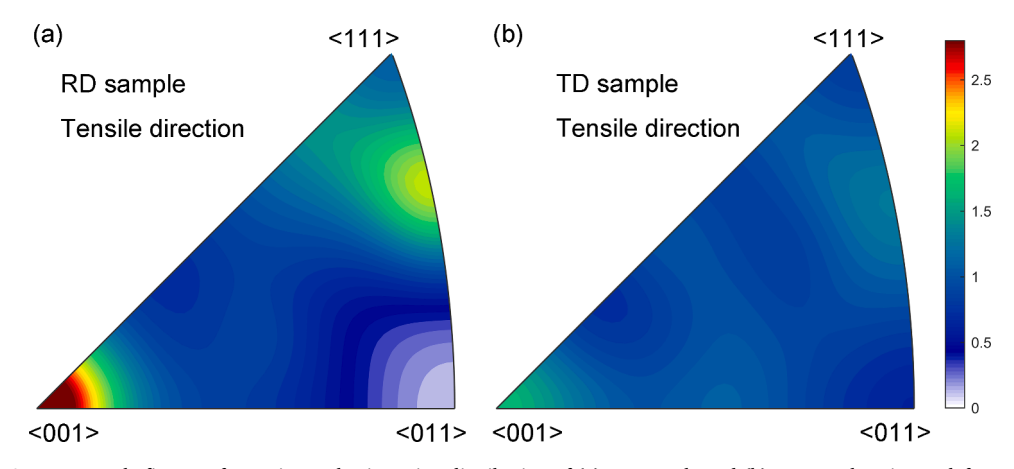


Fig. 6. Inverse pole figures of experimental orientation distribution of (a) RD sample and (b) TD sample prior to deformation.

fraction of grains shows a decrease of Von Mises stress around the average value 19.5 MPa, a subset of 10.4% grains exhibits a much higher stress reduction, ranging from 22.8 MPa to 27.2 MPa, as marked in Fig. 4(c). This suggests that some grains are experiencing stronger UA effect than the average. Pinpointing this subset and investigating the mechanism of higher stress reduction is necessary to better elucidate the mechanisms behind ultrasonic softening.

4.2. Orientation dependency of ultrasonic softening

As shown in Fig. 4(c), the softening behavior induced by ultrasound is not uniform across all grains according to the modeling analysis. The origin of this difference is further investigated in this section. The discrete experimental orientation data used as VPSC input for the TD test is plotted in tensile axis (TD) inverse pole figure, shown in Fig. 5(a). This map is color coded by the magnitude of Von Mises stress reduction calculated from VPSC modeling. A clear dependence of stress reduction on initial orientation can be observed. Stress reduction is the highest for $\langle 111 \rangle$ grains, followed by $\langle 001 \rangle$ grains with stress reduction of around 20 MPa. The magnitude of stress reduction decreases as orientation deviates. The lowest stress reduction occurs on $\langle 011 \rangle$ grains. The original texture of the 10.4% grains that show higher stress reduction, i.e., stress reduction of 22.8 MPa and above, is illustrated in Fig. 5(b) with orange markers. VPSC model shows that after tensile deformation with 17% strain, these grains rotate further towards the $\langle 111 \rangle$ direction, as shown by the blue markers.

The dependence of stress reduction on texture explains the difference in softening between RD and TD samples. Fig. 6(a) and (b) shows the original texture of copper foil along RD and TD directions, respectively. Higher intensities in both $\langle 111 \rangle$ and $\langle 001 \rangle$ grains are observed for RD sample. Since UA softening is more effective on these grains, especially $\langle 111 \rangle$ grains, macroscopically higher stress reduction is expected in the RD sample, which is in good agreement with experiment. As measured in Fig. 2(a), at 17% true strain, the stress reduction in the RD and TD sample is 31.8 MPa and 27.5 MPa respectively.

Based on these modeling insights, postmortem EBSD scans were performed on TD samples tested to 17% strain, both without and with UA, to study the microstructural evolution. From the experimental EBSD data, a subset with 15° tolerance to $\langle 111 \rangle$ on deformed specimen is extracted as the high stress reduction grain aggregate. It is revealed that these grains are the ones with high Taylor factors, as shown in Fig. 7. Taylor factor maps without and with UA are shown in Fig. 7(a) and (c). The corresponding Taylor factor maps of the extracted subset are shown in Fig. 7(b) and (d), respectively. Taylor factor is an orientation factor which depends on the orientation of a grain and the crystallographic nature of slip systems (Zhang et al., 2019). Lower Taylor factor indicates less energy is necessary to plastically deform a crystal of a given orientation (Bunge, 1970). While grains in the entire dataset have Taylor factors ranging from 2.29 to 3.66, this subset shows significantly higher Taylor factor values from 3.20 to 3.66. Combined with the modeling results that the grain subset closer to $\langle 111 \rangle$ directions have larger stress reduction; this suggests that a higher stress reduction occurs primarily in grains with plastically hard orientations.

5. Discussion

5.1. Change in Taylor factor in high stress reduction grains

Taylor factor is used as a metric to validate model prediction against experimental measurement. Taylor factor connects the magnitude of microscopic shear strain and macroscopic strain by: $m = \Sigma \gamma / \varepsilon_{VM}$ where $\Sigma \gamma$ is the sum of shear strain from slip in a grain, and ε_{VM} is the Von Mises equivalent macroscopic strain (Raabe et al., 2001; Zhang et al., 2020). It can also be written as the ratio between macroscopic stress σ_{VM} and the critical resolved shear stress $\hat{\tau}$: $m = \sigma_{VM}/\hat{\tau}$. Multiplying $d\varepsilon_{VM}$ to both the numerator and denominator gives:

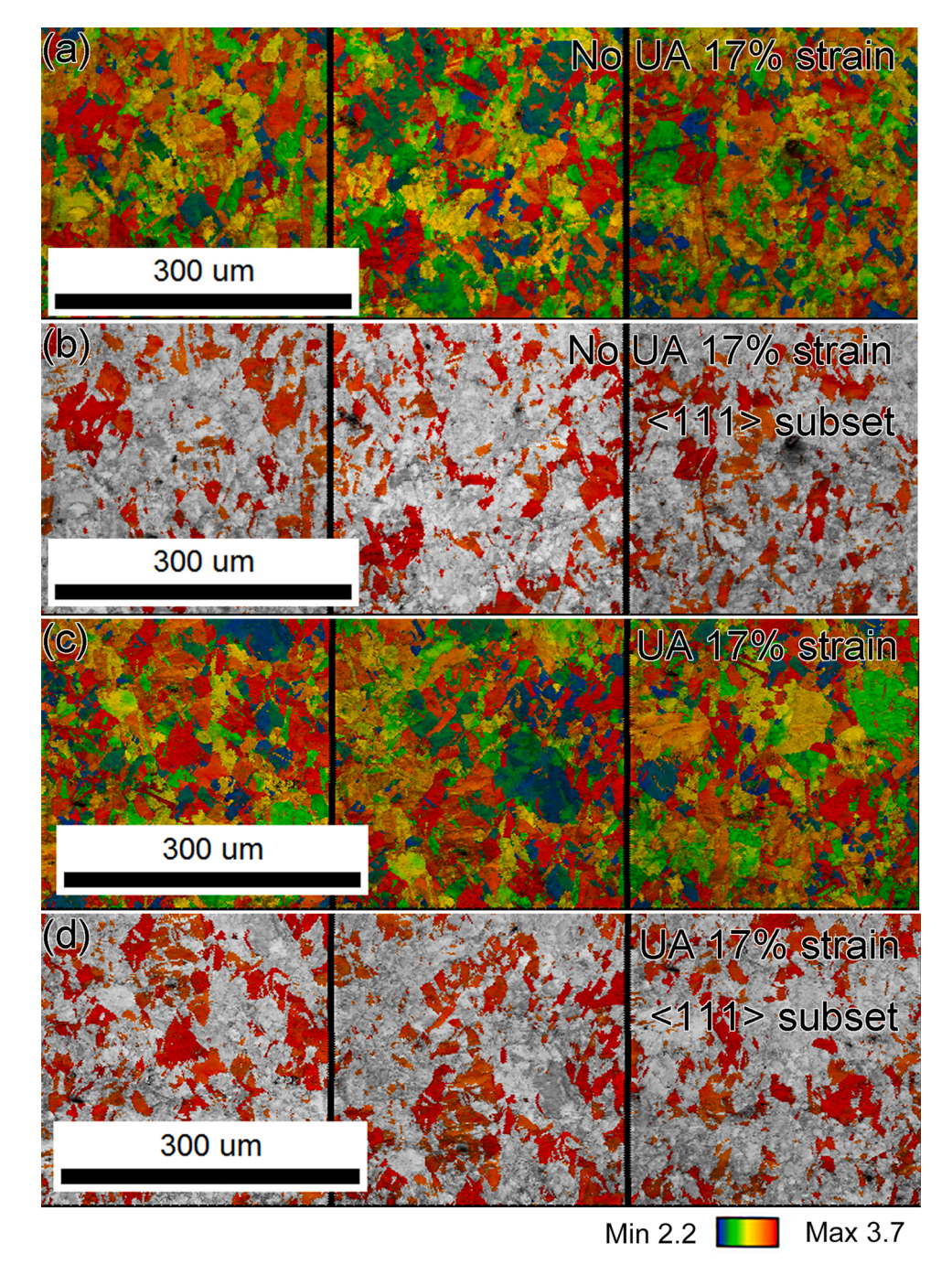


Fig. 7. Taylor factor map of TD samples (a) 17% strain no UA; (c) 17% strain UA; (b) and (d) are corresponding Taylor factor maps of (111) subset.

$$m = \frac{dW}{\hat{\tau} \cdot d\varepsilon_{VM}} = \frac{\sigma : \dot{\varepsilon}}{\hat{\tau} \cdot \dot{\varepsilon}_{VM}}$$
 (22)

where W is the plastic work, σ is the deviatoric stress tensor for individual grain, $\dot{\epsilon}$ is the imposed strain rate tensor, and $\dot{\epsilon}_{VM}$ is the Von Mises equivalent strain rate which is expressed as: $\dot{\epsilon}_{VM} = \sqrt{2/3\dot{\epsilon}_{ij}\dot{\epsilon}_{ij}} = \sqrt{2/3\dot{\epsilon}}$. Eq. (22) can then be written as Kocks et al. (1998), Lebensohn and Tomé (2015):

$$m = \sqrt{\frac{3\sigma : \dot{\varepsilon}}{2\hat{\tau} \cdot \parallel \dot{\varepsilon} \parallel}}$$
 (23)

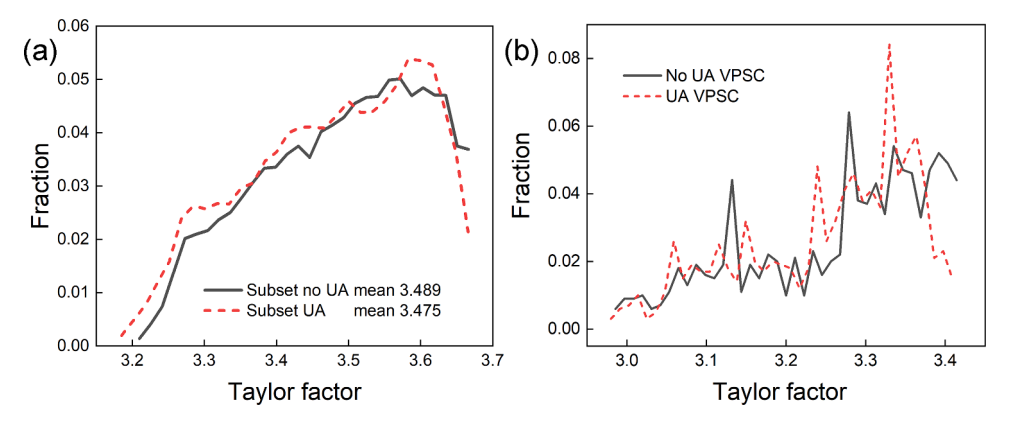


Fig. 8. Taylor factor distribution of the orientation subset for samples with no UA and UA (a) EBSD measurement and (b) VPSC simulation.

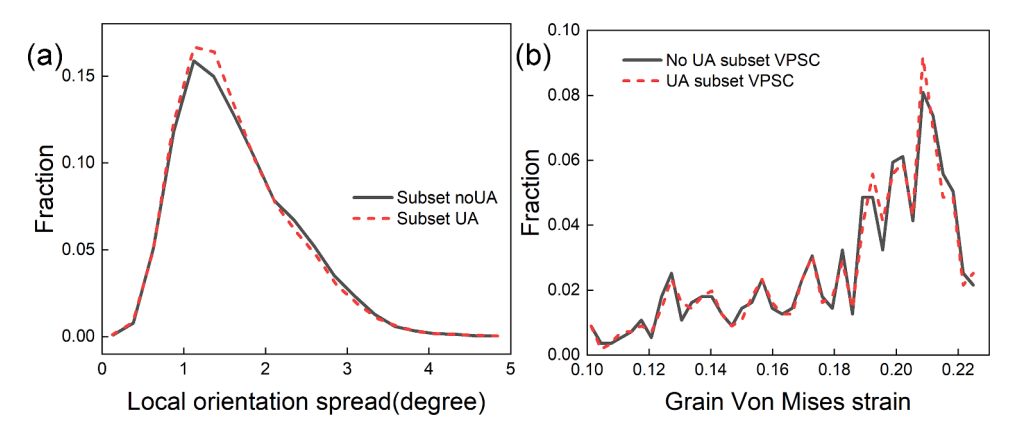


Fig. 9. Strain in $\langle 111 \rangle$ subset in (a) local orientation spread from EBSD measurement and (b) VPSC.

VPSC calculates Taylor factor for each grain using its stress state following Eq. (23). Taylor factor in EBSD is computed in OIM software based on the macroscopic strain and the orientation of grains. The histograms of experimental Taylor factor distribution for the grain subset in Fig. 7(b) and (d) are shown in Fig. 8(a). The distribution of Taylor factor with UA, shown in red dashed curve, shifts toward lower values compared to the one without UA (black solid curve). Drop in fractions of high Taylor factor grains is observed. The average Taylor factor in the extracted subset decreased from 3.489 to 3.475 with UA. Fig. 8(b) compares VPSC simulated distribution of Taylor factor for the high stress reduction (111) subset. Distinct decrease in high Taylor factor grains can be observed in the UA condition. The average of Taylor factor reduces from 3.273 to 3.257, which is in good agreement with the amount of reduction observed in EBSD measurement. On the other hand, it is noticeable that VPSC predicts a lower Taylor factor range than EBSD data processed by OIM software. This discrepancy originates from the different algorithms used in Taylor factor calculation. VPSC calculates Taylor factor of a grain from its individual stress condition and either 6 or 8 slip systems are activated in each grain. In comparison, OIM performs the calculation by finding a set of 5 slip systems that are activated based on the minimum work principle. Overall, the decrease in Taylor factor with UA from both experimental EBSD data and VPSC modeling predictions indicates that the orientation of grains has changed so that less macroscopic stress is needed for plastic deformation. Zhou et al. reported similar experimental observations on aluminum (Zhou et al., 2018). In their setup, ultrasonic vibration was also applied along the loading direction. A lower Taylor factor was observed in UA compression tests, which is attributed to ultrasonically induced grain reorientation.

Local misorientations provide an indication of the strain distribution in the material (Wright et al., 2011). The distribution of local orientation spread, in the same subsets, were extracted and shown in Fig. 9(a). Only minor differences are observed with UA, shown in red dashed curve, suggesting that strain level in these subsets is very similar. This is in good agreement with simulated grain Von Mises strain distribution of $\langle 111 \rangle$ subset, as shown in Fig. 9(b). Furthermore, it suggests that the change in Taylor factor shown in Fig. 8 is the result of applied ultrasonic vibration since the strain distribution among grains are the same.

In FCC metal, a classical analysis predicts a set of either 6 or 8 slip systems being activated in each grain (Bishop and Hill, 1951). Therefore, there are multiple ways of selecting slip systems to reach the same overall strain. A change in Taylor factor at the same strain level suggests that the selection of slip system has changed under UA in the grains that experienced significant softening. This will result in a change in rotation and final orientation in this set of grains. Given that these grains are a small fraction of the overall microstructure, the effect cannot be resolved from the effective or macroscale texture, however it is significant within a local grain

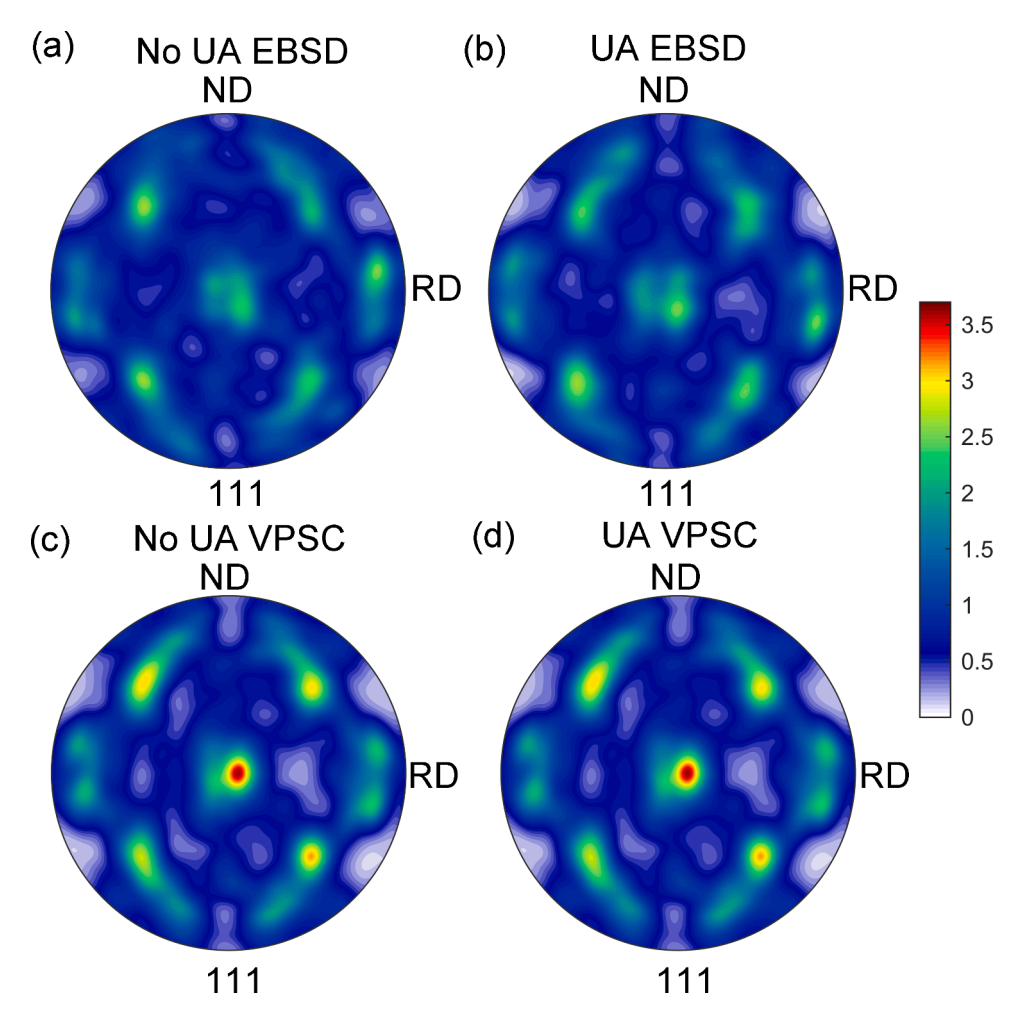


Fig. 10. {111} pole figure of pure copper TD samples with 17% tensile strain: (a) no UA EBSD; (b) UA EBSD; (c) no UA VPSC; (d) UA VPSC.

neighborhood. Analysis on VPSC slip system selection was performed but did not yield a clear pattern. A 3D full-field simulation is necessary to tease out these local microstructure effects and will be conducted in future studies.

5.2. Texture evolution

Texture of the TD specimen at 17% tensile strain without and with UA are measured using EBSD and compared with the predictions of VPSC softening models. Fig. 10 compares {111} pole figures with tensile direction pointing out of plane. Fig. 10(a) and (b) show {111} pole figures without and with UA from EBSD measurement. The corresponding modeling results are shown in Fig. 10(c) and (d). For FCC polycrystal materials, the strong pole in {111} can be observed in tensile direction (Bronkhorst et al., 1992). Here in this study, the applied true strain is limited to 17% so that strain distribution is still uniform along sample before necking starts to occur. As a result, some regions with high intensity from the original texture can still be clearly seen. Even though a reduction in Taylor factor with UA is observed in EBSD and VPSC softening model, which indicates that some grains have rotated differently under ultrasonic effect, no significant difference can be observed in the macroscale texture intensities in either EBSD or VPSC results of the whole aggregate. This is attributed to the fact FCC texture is mostly driven by overall deformation kinematics. In addition, UA effect is most significant on grains with high Taylor factors. Therefore, on a statistical level, no significant change in the texture of the whole aggregate is observed. The difference is clearer in high Taylor factor grains, as shown in Fig. 8. Lastly in Fig. 10, it is noticed that although modeling result agrees well with experiments qualitatively, it overpredicts texture intensity. Overprediction of texture intensity from VPSC model has been commonly reported in literature (Agnew et al., 2005; Field et al., 2002).

5.3. Comparison between directional and isotropic softening models

As a comparison, an isotropic softening model where the CRSS of every slip system is reduced by the same amount, is also established in this study. This is achieved by assigning the softening factor k in Eq. (15) to be a constant. Following the procedure from

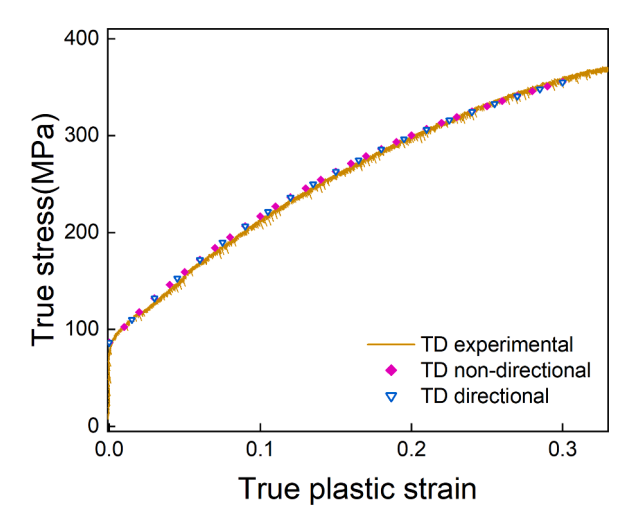


Fig. 11. Stress-strain data of UA tests simulated by directional and isotropic softening model.

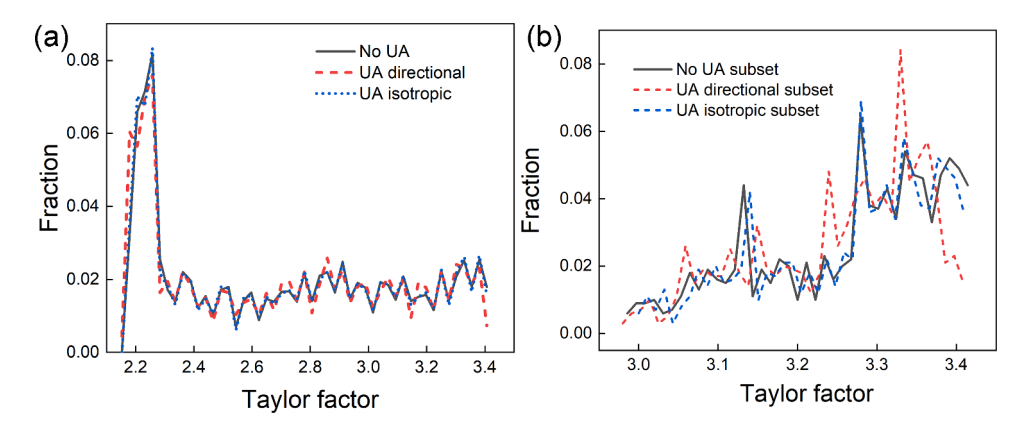


Fig. 12. Taylor factor distribution with 17% tensile strain from VPSC model with no UA, directional UA, and isotropic UA for (a) the entire aggregate and (b) (111) subset.

the directional model study, this isotropic model is first calibrated using the RD UA curve and then applied to predict the stress-strain response in the TD sample with UA. The softening factor k is fitted as 0.9991 from the RD UA tested stress-strain data. The Voce parameters are kept the same as in the directional model. The isotropic UA softening modeled TD stress strain curve is shown in Fig. 11 in blue triangles, which is compared with directional model prediction as well as experimental data on the same figure. It can be observed that the isotropic softening model also captures the stress-strain response reasonably well with the TD texture input under UA. The stress-strain predictions between isotropic and directional softening models are almost identical.

While the isotropic softening model can predict stress-strain responses under different initial textures, it fails to capture the changes in Taylor factor and grain level reorientation. Fig. 12 compares the simulated distribution of Taylor factor at 17% tensile strain with no UA, UA modeled using directional and isotropic softening methods. The histograms of Taylor factor of all grains and $\langle 111 \rangle$ subset is shown in Fig. 12(a) and (b), respectively. Over the whole grain assembly, little deviation of Taylor factor is observed between isotropic UA model and no UA condition in Fig. 12(a). In contrast, there are distinct changes in high and low Taylor factor grains in the directional UA softening model. In the subset of grains that show the most significant reduction in Von Mises stress, the difference between the isotropic and the directional softening model is clearer, as shown in Fig. 12(b). While a decrease in the fraction of high Taylor factor grains can be noticed in the directional model, the Taylor factor predicted by the isotropic model mostly overlaps with no UA condition, which does not match with experimental observation shown in Fig. 8(a).

In existing experimental studies of ultrasonic softening during metal plasticity, the degree of flow stress reduction as well as the homogeneity of stress reduction in the whole aggregate were not discussed. Here with the aid of crystal plasticity modeling, it is revealed that stress reduction is not homogenous among grains and that those grains with a high Taylor factor undergo higher stress reduction. Since Taylor factor is a measure of energy necessary to deform a crystal of a certain orientation (Bunge, 1970), this suggests that UA is more effective on the hard orientations. While existing crystal plasticity models can capture the reduction in flow stress, they do not show changes in Taylor factor. The directional softening proposed in this study can predict a decrease in Taylor factor at a similar level as experimentally measured by EBSD. This provides fresh insight into the mechanism of the ultrasonic softening

phenomenon and the effect of anisotropic softening in slip systems.

6. Conclusion

A novel approach to modeling ultrasonic softening effect is proposed by considering the orientation relationship between static loading and ultrasonic vibration. The effect of ultrasonic vibration on dislocation slip is assumed to be the most significant for the slip system orientated in the same direction as the ultrasonic vibration. The directional softening model was implemented in VPSC and validated with micro-tensile tests of pure copper. Stress-strain data from the model match well with experiment. Statistical analysis on grain level shows that Von Mises stress on all grains decrease under UA while insignificant change is observed in grain Von Mises strain. It is revealed for the first time that the level of Von Mises stress reduction varies among grains and shows a strong dependence on grain orientation. In a tensile test with ultrasonic vibration along the loading direction, (111) grains parallel to the tensile direction undergo the highest amount of stress reduction. EBSD analysis reveals that those grains originally have high Taylor factors are plastically hard for deformation with multislip. A relative decrease in Taylor factor in those grains is observed with UA and matches with model prediction. On the other hand, the reorientation of these grains shows minimal effects on the overall texture of the tested sample since the volume fraction of those grains is small. As a comparison to the directional softening model proposed in this study, an isotropic softening model using existing method was also run. While the latter can predict the change in stress-strain behavior, it fails to predict the change in Taylor factor under UA. The directional model proposed in this study provides new insights into the mechanism of ultrasonic softening effect. I is worth noting that there are limitations of VPSC as a mean-field method. The prediction that all grains undergoing stress reduction might be unrealistic because of local compatibility. A full-field crystal plasticity model will be set up for further investigation in future work.

CRediT authorship contribution statement

Jiarui Kang: Conceptualization, Methodology, Formal analysis, Investigation, Validation, Software, Visualization, Writing – original draft. **Xun Liu:** Conceptualization, Methodology, Formal analysis, Software, Visualization, Writing – review & editing, Supervision. **Stephen R. Niezgoda:** Conceptualization, Methodology, Formal analysis, Software, Visualization, Writing – review & editing, Supervision.

Declaration of Competing Interest

The authors declare that they have no known competing financial interests or personal relationships that could have appeared to influence the work reported in this paper.

Acknowledgements

This work was supported by National Science Foundation CMMI AM program [grant number: 2019238]. Electron microscopy was performed at the Center for Electron Microscopy and Analysis (CEMAS) at The Ohio State University. The authors are thankful to Dr. C. Tomé for providing VPSC code. Helpful discussion with Dr. S. Wright from EDAX is also appreciated.

References

- Agnew, S.R., Mehrotra, P., Lillo, T.M., Stoica, G.M., Liaw, P.K., 2005. Texture evolution of five wrought magnesium alloys during route A equal channel angular extrusion: experiments and simulations. Acta Mater. 53, 3135–3146. https://doi.org/10.1016/j.actamat.2005.02.019.
- Bagherzadeh, S., Abrinia, K., 2015. Effect of ultrasonic vibration on compression behavior and microstructural characteristics of commercially pure aluminum. J. Mater. Eng. Perform. 24, 4364–4376. https://doi.org/10.1007/s11665-015-1730-8.
- Bishop, J.F.W., Hill, R., 1951. CXXVIII. A theoretical derivation of the plastic properties of a polycrystalline face-centred metal. London, Edinburgh, Dublin. Philos. Mag. J. Sci. 42, 1298–1307. https://doi.org/10.1080/14786444108561385.
- Bronkhorst, C.A., Kalidindi, S.R., Anand, L., 1992. Polycrystalline plasticity and the evolution of crystallographic texture in FCC metals. Philos. Trans. R. Soc. London. Ser. A Phys. Eng. Sci. 341, 443–477. https://doi.org/10.1098/rsta.1992.0111.
- Bunge, H.J., 1970. Some applications of the Taylor theory of polycrystal plasticity. Krist. Tech. 5, 145–175. https://doi.org/10.1002/crat.19700050112.
- Cao, M.Y., Hu, H., Jia, X.D., Tian, S.J., Zhao, C.C., Han, X.B., 2020. Mechanism of ultrasonic vibration assisted upsetting of 6061 aluminum alloy. J. Manuf. Process. 59, 690–697. https://doi.org/10.1016/j.jmapro.2020.09.070.
- Choi, I.-.C., Kim, Y.-.J., Ahn, B., Kawasaki, M., Langdon, T.G., Jang, J., 2014. Evolution of plasticity, strain-rate sensitivity and the underlying deformation mechanism in Zn–22% Al during high-pressure torsion. Scr. Mater. 75, 102–105. https://doi.org/10.1016/j.scriptamat.2013.12.003.
- Deshpande, A., Hsu, K., 2018. Acoustic energy enabled dynamic recovery in aluminium and its effects on stress evolution and post-deformation microstructure. Mater. Sci. Eng. A 711, 62–68. https://doi.org/10.1016/j.msea.2017.11.015.
- Dukhin, A.S., Goetz, P.J., 2017. Chapter 3 Fundamentals of acoustics in homogeneous liquids: longitudinal rheology. In: Dukhin, A.S. (Ed.), Goetz Dispersions, Emulsions, and Porous Materials Using Ultrasound (Third Edition), P.J.B.T.-C. of L. Elsevier, pp. 85–118. https://doi.org/10.1016/B978-0-444-63908-0.00003-X.
- Dutta, R.K., Petrov, R.H., Delhez, R., Hermans, M.J.M., Richardson, I.M., Böttger, A.J., 2013. The effect of tensile deformation by in situ ultrasonic treatment on the microstructure of low-carbon steel. Acta Mater 61, 1592–1602. https://doi.org/10.1016/j.actamat.2012.11.036.
- Fartashvand, V., Abdullah, A., Sadough Vanini, S.A., 2017. Investigation of Ti-6Al-4V alloy acoustic softening. Ultrason. Sonochem. 38, 744–749. https://doi.org/10.1016/j.ultsonch.2016.07.007.
- Field, R.D., Hartwig, K.T., Necker, C.T., Bingert, J.F., Agnew, S.R., 2002. Equal-channel angular extrusion of beryllium. Metall. Mater. Trans. A 33, 965–972. https://doi.org/10.1007/s11661-002-0166-6.
- Graff, K.F., 2015. 14 Ultrasonic Metal Forming: Materials, in: Gallego-Juárez, J.A., Graff, K.F.B.T.-P.U., Woodhead Publishing, Oxford, pp. 337–376. 10.1016/B978-1-78242-028-6.00014-4.

Groche, P., Schäfer, R., Justinger, H., Ludwig, M., 2010. On the correlation between crystallographic grain size and surface evolution in metal forming processes. Int. J. Mech. Sci. 52, 523–530. https://doi.org/10.1016/j.ijmecsci.2009.11.017.

Hielscher, R., Schaeben, H., 2008. A novel pole figure inversion method: specification of the {\it MTEX} algorithm. J. Appl. Crystallogr. 41, 1024–1037. https://doi.org/10.1107/S00218898030112.

Kang, J., Liu, X., Xu, M., 2020. Plastic deformation of pure copper in ultrasonic assisted micro-tensile test. Mater. Sci. Eng. A 785, 139364. https://doi.org/10.1016/j.msea.2020.139364.

Kocks, U.F., Tomé, C.N., Wenk, H.-.R., 1998. Texture and anisotropy: Preferred Orientations in Polycrystals and Their Effect On Materials Properties. Cambridge university press.

Lebensohn, R.A., Tomé, C.N., 2015. Manual for Code Visco-Plastic Self-Consistent (VPSC), Version 7d.

Lebensohn, R.A., Tomé, C.N., 1993. A self-consistent anisotropic approach for the simulation of plastic deformation and texture development of polycrystals: application to zirconium alloys. Acta Metall. Mater. 41, 2611–2624. https://doi.org/10.1016/0956-7151(93)90130-K.

Maloney, K.J., Roper, C.S., Jacobsen, A.J., Carter, W.B., Valdevit, L., Schaedler, T.A., 2013. Microlattices as architected thin films: analysis of mechanical properties and high strain elastic recovery. APL Mater 1. https://doi.org/10.1063/1.4818168.

Malygin, G.A., 2000. Acoustoplastic effect and the stress superimposition mechanism. Phys. Solid State 42, 72-78. https://doi.org/10.1134/1.1131170.

Mao, Q., Coutris, N., Rack, H., Fadel, G., Gibert, J., 2020. Investigating ultrasound-induced acoustic softening in aluminum and its alloys. Ultrasonics 102, 106005. https://doi.org/10.1016/j.ultras.2019.106005.

Mariani, E., Ghassemieh, E., 2010. Microstructure evolution of 6061 O Al alloy during ultrasonic consolidation: an insight from electron backscatter diffraction. Acta Mater. 58, 2492–2503. https://doi.org/10.1016/j.actamat.2009.12.035.

Peach, M., Koehler, J.S., 1950. The forces exerted on dislocations and the stress fields produced by them. Phys. Rev. 80, 436–439. https://doi.org/10.1103/PhysRev.80.436.

Prabhakar, A., Verma, G.C., Krishnasamy, H., Pandey, P.M., Lee, M.G., Suwas, S., 2017. Dislocation density based constitutive model for ultrasonic assisted deformation. Mech. Res. Commun. 85, 76–80. https://doi.org/10.1016/j.mechrescom.2017.08.003.

Raabe, D., Sachtleber, M., Zhao, Z., Roters, F., Zaefferer, S., 2001. Micromechanical and macromechanical effects in grain scale polycrystal plasticity experimentation and simulation. Acta Mater 49, 3433–3441. https://doi.org/10.1016/S1359-6454(01)00242-7.

Rout, M., 2020. Texture-tensile properties correlation of 304 austenitic stainless steel rolled with the change in rolling direction. Mater. Res. Express 7. https://doi.org/10.1088/2053-1591/ab677c.

Sedaghat, H., Xu, W., Zhang, L., 2019. Ultrasonic vibration-assisted metal forming: constitutive modelling of acoustoplasticity and applications. J. Mater. Process. Technol. 265, 122–129. https://doi.org/10.1016/j.jmatprotec.2018.10.012.

Siddiq, A., Sayed, T.El, 2012a. A thermomechanical crystal plasticity constitutive model for ultrasonic consolidation. Comput. Mater. Sci. 51, 241–251. https://doi.org/10.1016/j.commatsci.2011.07.023.

Siddiq, A., Sayed, T.El, 2012b. A thermomechanical crystal plasticity constitutive model for ultrasonic consolidation. Comput. Mater. Sci. 51, 241–251. https://doi.org/10.1016/j.commatsci.2011.07.023.

Siddiq, A., Sayed, T.El, 2011. Acoustic softening in metals during ultrasonic assisted deformation via CP-FEM. Mater. Lett. 65, 356–359. https://doi.org/10.1016/j.matlet.2010.10.031.

Siu, K.W., Ngan, A.H.W., 2013. Oscillation-induced softening in copper and molybdenum from nano- to micro-length scales. Mater. Sci. Eng. A 572, 56–64. https://doi.org/10.1016/j.msea.2013.02.037.

Siu, K.W., Ngan, A.H.W., 2011. Understanding acoustoplasticity through dislocation dynamics simulations. Philos. Mag. 91, 4367–4387. https://doi.org/10.1080/14786435.2011.606237.

Siu, K.W., Ngan, A.H.W., Jones, I.P., 2011. New insight on acoustoplasticity - Ultrasonic irradiation enhances subgrain formation during deformation. Int. J. Plast. 27, 788–800. https://doi.org/10.1016/j.ijplas.2010.09.007.

Sridhar, S.K., Stebner, A.P., Rollett, A.D., 2022. Plastic deformation mechanisms that explain hot-rolling textures in Nickel–Titanium. Int. J. Plast. 153, 103257. https://doi.org/10.1016/j.ijplas.2022.103257.

https://doi.org/10.1016/j.ipplas.2022.103257.
Wang, C.J., Liu, Y., Guo, B., Shan, D.B., Zhang, B., 2016. Acoustic softening and stress superposition in ultrasonic vibration assisted uniaxial tension of copper foil: experiments and modeling. Mater. Des. 112, 246–253. https://doi.org/10.1016/j.matdes.2016.09.042.

Wang, X., Wang, C., Liu, Y., Liu, C., Wang, Z., Guo, B., Shan, D., 2021. An energy based modeling for the acoustic softening effect on the Hall-Petch behavior of pure titanium in ultrasonic vibration assisted micro-tension. Int. J. Plast. 136, 102879 https://doi.org/10.1016/j.ijplas.2020.102879.

Wright, S.I., Nowell, M.M., Field, D.P., 2011. A review of strain analysis using electron backscatter diffraction. Microsc. Microanal. 17, 316–329. https://doi.org/10.1017/S1431927611000055.

Yang, C.L., Wu, C.S., 2019. Constitutive equation with residual hardening effect for modeling the ultrasonic vibration enhanced friction stir welding process. Sci. Technol. Weld. Join. 24, 695–705. https://doi.org/10.1080/13621718.2019.1594586.

Yao, Z., Kim, G.Y., Wang, Z., Faidley, L.A., Zou, Q., Mei, D., Chen, Z., 2012. Acoustic softening and residual hardening in aluminum: modeling and experiments. Int. J. Plast. 39, 75–87. https://doi.org/10.1016/j.ijplas.2012.06.003.

Zhang, K., Holmedal, B., Mánik, T., Saai, A., 2019. Assessment of advanced Taylor models, the Taylor factor and yield-surface exponent for FCC metals. Int. J. Plast. 114, 144–160. https://doi.org/10.1016/j.iiplas.2018.10.015.

Zhang, W., Wang, X., Wang, Y., Yu, X., Gao, Y., Feng, Z., 2020. Type IV failure in weldment of creep resistant ferritic alloys: II. Creep fracture and lifetime prediction.

J. Mech. Phys. Solids 134, 103775. https://doi.org/10.1016/j.jmps.2019.103775.

Zhao, W., Wu, C., 2019. Constitutive equation including acoustic stress work and plastic strain for modeling ultrasonic vibration assisted friction stir welding process. Int. J. Mach. Tools Manuf. 145, 103434. https://doi.org/10.1016/j.ijmachtools.2019.103434.

Zhou, H., Cui, H., Qin, Q.H., 2018. Influence of ultrasonic vibration on the plasticity of metals during compression process. J. Mater. Process. Technol. 251, 146–159. https://doi.org/10.1016/j.jmatprotec.2017.08.021.

Zhuang, X.C., Wang, J.P., Zheng, H., Zhao, Z., 2015. Forming mechanism of ultrasonic vibration assisted compression. Trans. Nonferrous Met. Soc. China (English Ed.) 25, 2352–2360. https://doi.org/10.1016/S1003-6326(15)63850-X.